

Supporting Information for:

Mobilisation of arsenic from bauxite residue (red mud) affected soils: Effect of pH and redox conditions.

Cindy L. Lockwood^{1§}, Robert J. G. Mortimer¹, Douglas I. Stewart², William M. Mayes³, Caroline L. Peacock¹, David A. Polya⁴, Paul R Lythgoe⁴, Alizée P. Lehoux^{1#}, Katalin Gruiz⁵ and Ian T. Burke^{1*}

¹School of Earth and Environment, University of Leeds, Leeds, LS2 9JT, UK. *Corresponding Author's E-mail: I.T.Burke@leeds.ac.uk; Phone: +44 113 3437532; Fax: +44 113 3435259

²School of Civil Engineering, University of Leeds, Leeds, LS2 9JT, UK.

³Centre for Environmental and Marine Sciences, University of Hull, Scarborough, YO11 3AZ, UK

⁴School of Earth, Atmospheric and Environmental Science and Williamson Research Centre for Molecular Environmental Science, University of Manchester, Manchester, UK

⁵Department of Applied Biotechnology and Food Science, Budapest University of Technology and Economics, 1111 Budapest, St Gellért sq. 4, Hungary

[§]Present address: Center for Applied Geoscience (ZAG), Eberhard-Karls-University Tuebingen, Sigwartstrasse 10, 72076 Tuebingen, Germany

[#]Present address: INRA, UMR1114EMMAH, F-84000 Avignon Laboratoire Navier, UMR8202, Université Paris-Est, Champs sur Marne, France

Prepared for Applied Geochemistry, 06 November 2014

This consists of two sections. Section 2.0 contains 6 figures and 1 table.

Section 1.0 XAS analysis.

1.1 XANES Detailed Method

Approximately 100 mg samples of moist red mud sample or soils recovered from microcosm experiments were prepared for XAS analysis by mounting under an argon atmosphere into in Perspex holders with Kapton™ windows. Samples were frozen (-20°C) and transported to the synchrotron on dry ice. Solutions of sodium arsenate (Na_3AsO_4) and sodium arsenite (Na_3AsO_3) were prepared at 1000 mg.L^{-1} [As] and held in polythene bags for analysis.

As K-edge spectra (11867 eV) were collected on beamline I18 at the Diamond Light Source operating at 3 GeV with a typical current of 200 mA, using a nitrogen cooled Si(111) double crystal monochromator and focussing optics. A pair of plane mirrors was used to reduce the harmonic content of the beam and Kirkpatrick-Baez mirrors were used to produce a relatively unfocused beam (approximately 0.5mm diameter at the sample). K-edge spectra were collected in fluorescence mode at room temperature ($\sim 295 \text{ °K}$) using a 9 element solid state Ge detector. As K-edge spectra from solid samples were found to be affected by beam damage presenting as an apparent change in As speciation that increased in magnitude with increased exposure to the beam (Charlet et al., 2011; Morin et al., 2008). To mitigate this effect, only single As K-edge EXAFS spectra were collected (~ 20 mins) from a spot within the sample and the sample stage automatically moved to expose an unaffected part of the sample before subsequent scans.

Multiple scans (9) were then averaged to improve the signal to noise ratio using Athena version 0.8.061 (Ravel and Newville, 2005). For XANES spectra absorption was also normalised in Athena over $0-8 \text{ \AA}^{-1}$ and then plotted from approximately -15 eV to +30 eV relative to the edge position with no correction required for drift in E_0 .

1.2 EXAFS Detailed Method

EXAFS data (collected from $0-14 \text{ \AA}^{-1}$) was background subtracted using PySpline v1.1 (Tenderholt et al., 2007) and analysed in DLExcurv v1.0 (Tomic, 2005) (from $3-14 \text{ \AA}^{-1}$) using full curved wave theory (Gurman et al., 1984). Phaseshifts were derived from *ab initio* calculations using Hedin-Lundqvist potentials and von-Barth ground states (Binsted, 1998). Multiple scattering was allowed for as coded in DLExcurv (Binsted, 1998; Tomic, 2005). Multiple scattering calculations require specification of the full three dimensional structure of the As coordination environment (i.e., bond

angles in addition to bond lengths). This was done using hypothetical model clusters with C_1 symmetry. The contribution of all possible multiple scattering paths within the AsO_4 tetrahedral were calculated by the software including the As-O-O (2.8 Å) and As-O-As-O paths (3.3 Å). The spectra for the red mud sample was then fit by refining each model cluster, and the best fit evaluated using the EXAFS R-factor (Binsted et al., 1992), the EXAFS Fit Index (as coded Binsted (1998)) and the reduced χ^2 values (as coded in EXCURV98 ((Binsted, 1998) and references therein)). Specifically, reduced χ^2 values were used to evaluate the fits of each experimental spectrum to various single shell (involving only nearest neighbour oxygens) vs. multiple shell (involving nearest neighbour oxygens and next-nearest neighbour Al) model clusters. In this way the statistical significance of invoking Al or Fe backscatters was determined. Next-nearest neighbour Al shells were only included if the reduced χ^2 was improved by $\geq 10\%$, compared to a single shell (oxygens only) cluster (Peacock, 2009). It should be noted that, in DLexcurv, the absolute value of reduced χ^2 is not accurate (as DLexcurv does not require actual experimental statistical errors). Rather, reduced χ^2 is used as a relative guide where a reduction or minimum indicates an improved fit. Fitting involved the refinement of an energy correction E_f (the Fermi Energy (or δE_0); which for final fits was $\sim -13.5 \pm 0.2$ eV), and the absorber-scatterer distance and the Debye-Waller factor for each shell. The amplitude factor (S_0^2 or AFAC in DLexcurv V1.0) was retained as the default of 1 throughout. During fitting the number of independent data points was always greater than the number of fitted parameters (in DLexcurv these are N_{ind} and N_{pars} , respectively). N_{ind} was determined using Stern's rule (Stern, 1993) as $2\Delta k\Delta R/\pi + 2$ (Booth and Hu, 2009) where Δk and ΔR are the range in k - and R -space actually fitted. All spectra were fit in k -space and no Fourier filtering was performed.

Fourier transforms of the EXAFS spectra were used to obtain an approximate radial distribution function around the central As atom (the absorber atom); the peaks of the Fourier transform can be related to "shells" of surrounding backscattering ions characterised by atom type, number of atoms, absorber-scatterer distance, and the Debye-Waller factor ($\pm 25\%$), $2\sigma^2$. Modelling As co-ordination without multiple scattering produced significantly poorer fits and did not account for the small peak observed at ~ 3.0 Å in the radial distribution function. The 2.8-3.0 Å peak has previously been incorrectly ascribed as a valid atomic backscattering distance (e.g. Manceau, 1995); however, when correctly including multiple scattering this peak can be accounted for (discussed at length in

Sherman and Randall, 2003). Atomic distances calculated by DLexcurv have a precision error of approximately ± 0.02 and ± 0.05 Å in the first and outer shells respectively (Burke et al., 2005). Debye-Waller factors are typically $0.002 - 0.02$ $2\sigma^2$ for the first shell and $0.02 - 0.04$ $2\sigma^2$ for the outer shells (Binsted, 1998).

Section 2.0 Figures and Tables

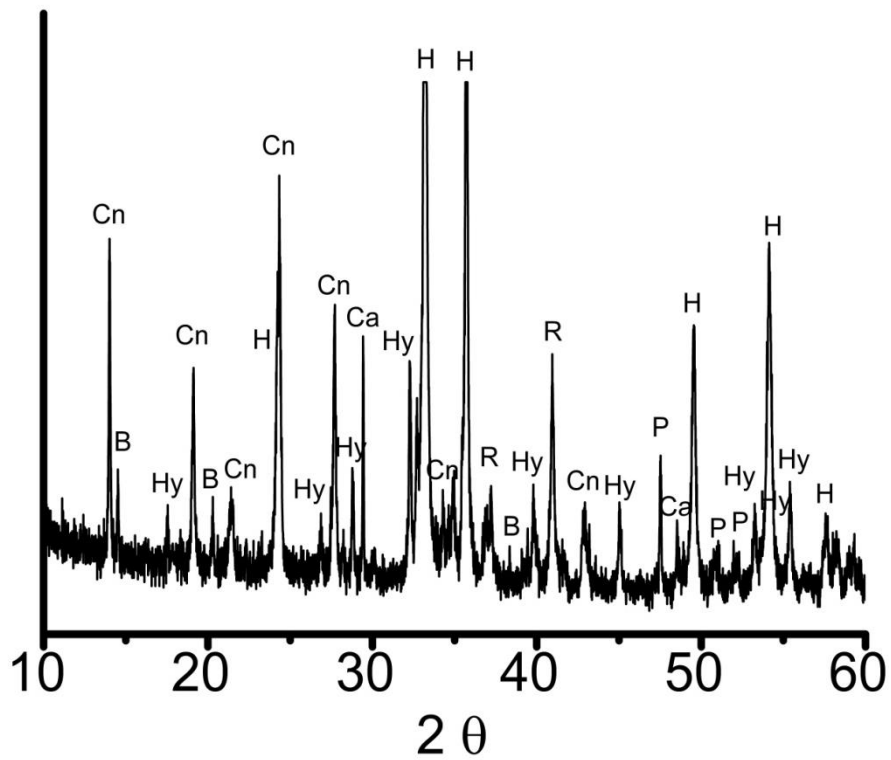


Figure S1. XRD pattern for red mud sampled from inside the breached tailings dam at Ajka.

B = boehmite, Ca = Calcite, Cn = cancrinite, H = hematite, Hy = hydrogarnet, P = perovskite, R = rutile

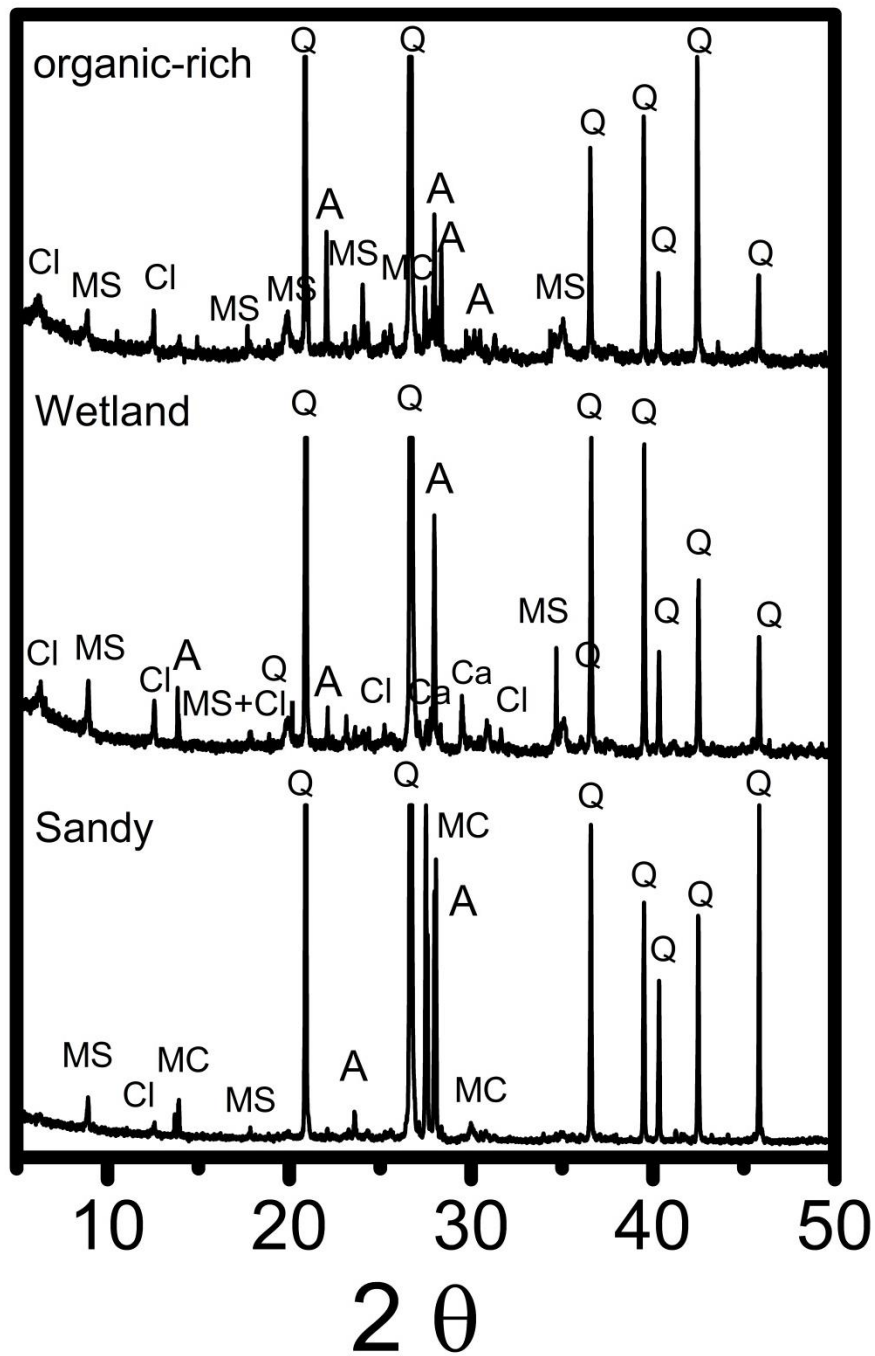


Figure S2. – XRD patterns of soils sampled from Torna-Marcel-Raba river system

A = albite, Ca = calcite, Cl = chlorite, Q = quartz, MC = microcline, MS = muscovite

Table S1. Full XRF analysis of red mud and soils

Concentrations of selected elements present in the red mud sample and soil samples prior to amendment.

Major Elements (Weight %Oxides)	Red Mud	Organic-rich soil	Wetland soil	Sandy soil
SiO ₂	12.9	72.9	80.6	89.8
TiO ₂	5.24	0.48	0.33	0.37
Al ₂ O ₃	16.0	8.9	6.4	4.2
Fe ₂ O ₃	38.5	3.0	1.8	1.7
MnO	0.31	0.04	0.03	0.06
MgO	0.61	0.84	0.98	0.06
CaO	8.0	1.0	2.27	0.60
Na ₂ O	8.0	1.0	0.90	0.71
K ₂ O	0.10	1.6	1.3	0.87
P ₂ O ₅	0.19	0.11	0.07	0.08
SO ₃	0.36	0.02	0.02	0.006
<i>LOI</i>	<i>8.0</i>	<i>10.2</i>	<i>5.1</i>	<i>1.8</i>
Minor Elements (mg kg ⁻¹)				
As	196	11	8	2
Ba	66	396	267	148
Ce	607	47	34	17
Co	59	11	5	3
Cr	864	68	62	50
Cu	104	12	6	2
Ga	26	10	6	4
La	283	26	18	10
Mo	15	1	1	1
Ni	361	23	14	5
Pb	215	25	12	9
Sb	22	1	2	1
Sr	318	78	94	47
Th	98	6	4	2
U	21	3	2	1
V	1132	72	51	30
W	17	<1	<1	<1
Zn	162	52	26	21
Zr	1223	122	102	88

< denotes less than given level of detection

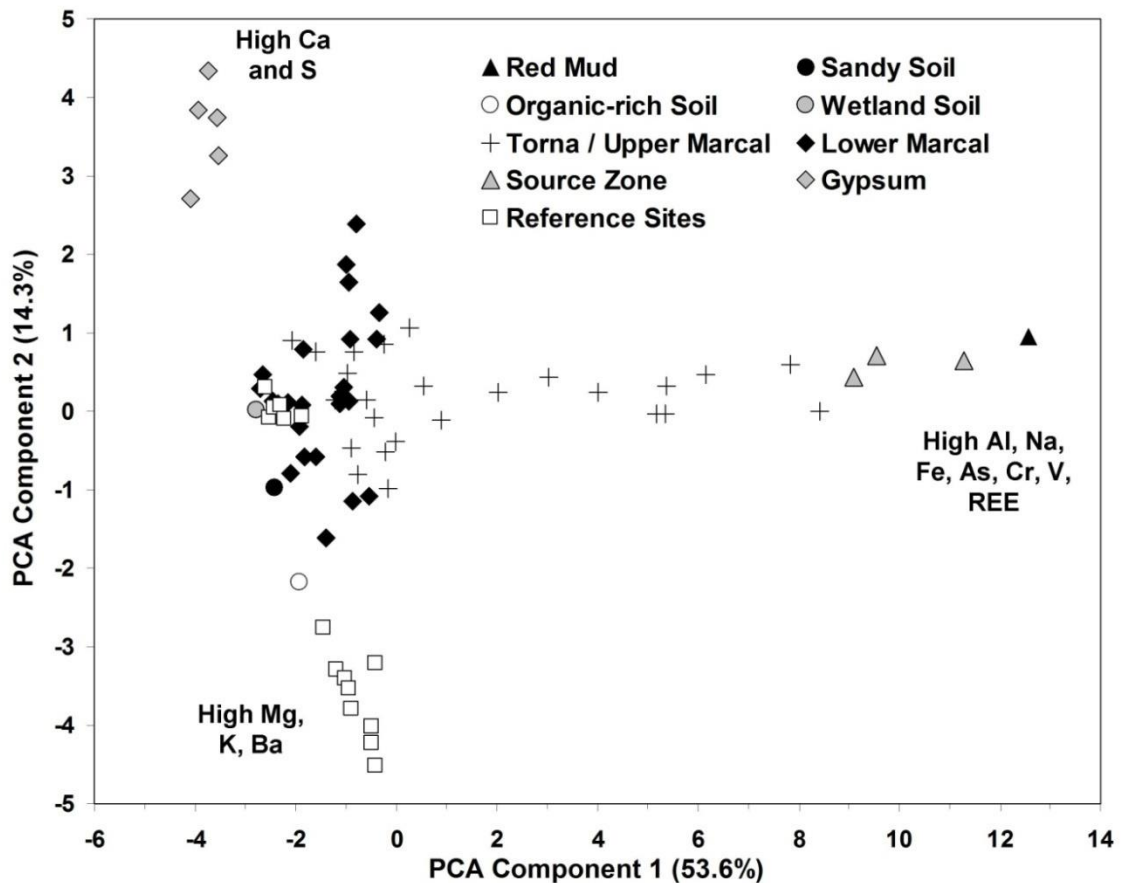


Figure S3. Principle Component Analysis - shows the samples used in this study in the broader context of large scale soil and sediment sampling efforts across a 100km reach of the Torna-Marcal-Raba River system in the immediate aftermath of the spill (Mayes et al., 2011). Each point represents a single sample station and three end members are apparent in the PCA. Samples of red mud from the Ajka repository plot at the extreme right hand side of the figure, being characterised by enriched Fe, Al, Ti, Na, Cr, V and various other trace elements. The red mud samples used in this study (labelled 'Red Mud' in the legend) plot alongside those red mud taken from previous sampling efforts at the same site (labelled 'Source', sample K1 from Mayes et al. (2011)). To the upper left of Figure S4, samples enriched with Ca and S are indicative of river sediments in reaches subject to extensive gypsum dosing (to neutralise the high pH) shortly after the spill. To the lower left, unaffected reference sites are apparent as a final end member and are relatively enriched in K, Ba and Mg, consistent with bedrock lithology (Mayes et al., 2011). The samples plotting between these end members represent mixing of these different extremes, for example the samples that plot in a roughly straight horizontal line from the red mud to the left hand side of Figure S4 represent dilution of red mud through mixing with soils and sediments with distance downstream from the source area. The soil samples used in this study all plot in a group on the left hand side with unaffected sites from the lower Marcal River and reference ('REF') samples showing them to be representative of the broad geochemical constituent of unaffected sediments in the Marcal catchment. The pH of the waters in this area are neutral (pH 7 – 8) as this area is dominated by dolomite and limestone bedrock (see Mayes et al. (2011)).

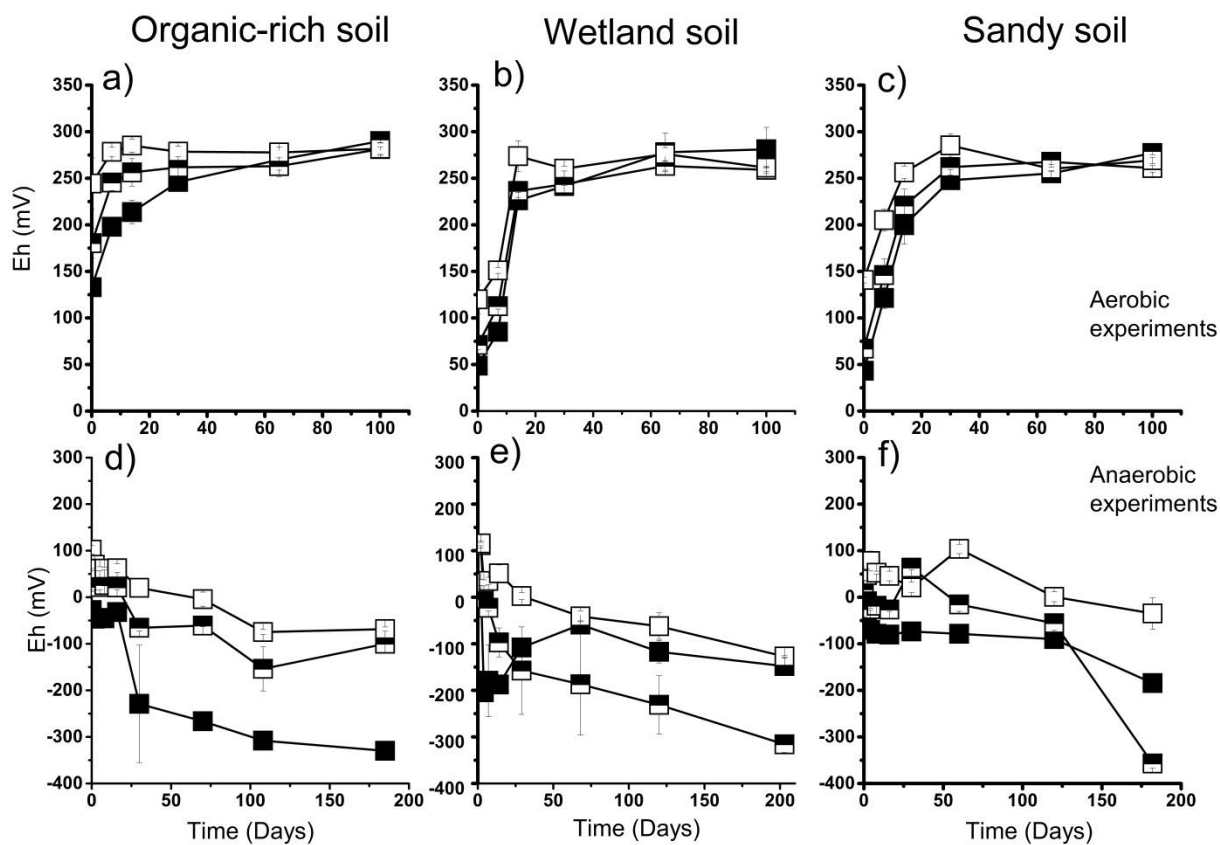


Figure S4. Geochemical analysis time plots from aerobic experiments (top graphs a-c) and anaerobic experiments (bottom graphs d-f) showing ORP (as an indicator for Eh). Empty squares = unamended, Half squares = 9% RM addition, Full squares = 33% RM addition. Error bars are 1 σ of triplicate results (where not shown, errors are within the symbol size). Please note the differences in both the x and y axes.

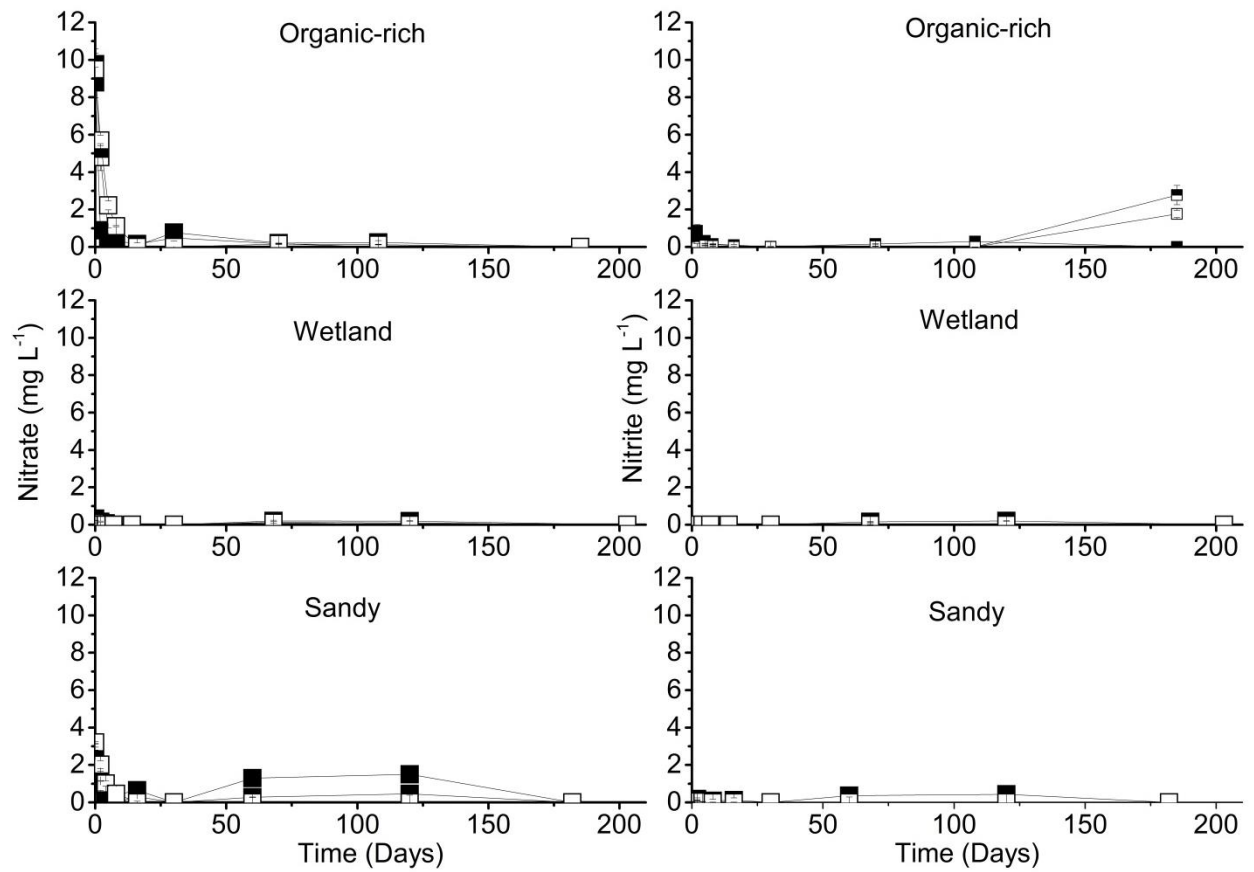


Figure S5. Nitrate and nitrite (mg L^{-1}) analysis time plots from anaerobic experiments. Empty squares = unamended, Half squares = 9% RM addition, Full squares = 33% RM addition. Error bars are 1σ of triplicate results (where not shown, errors are within the symbol size).

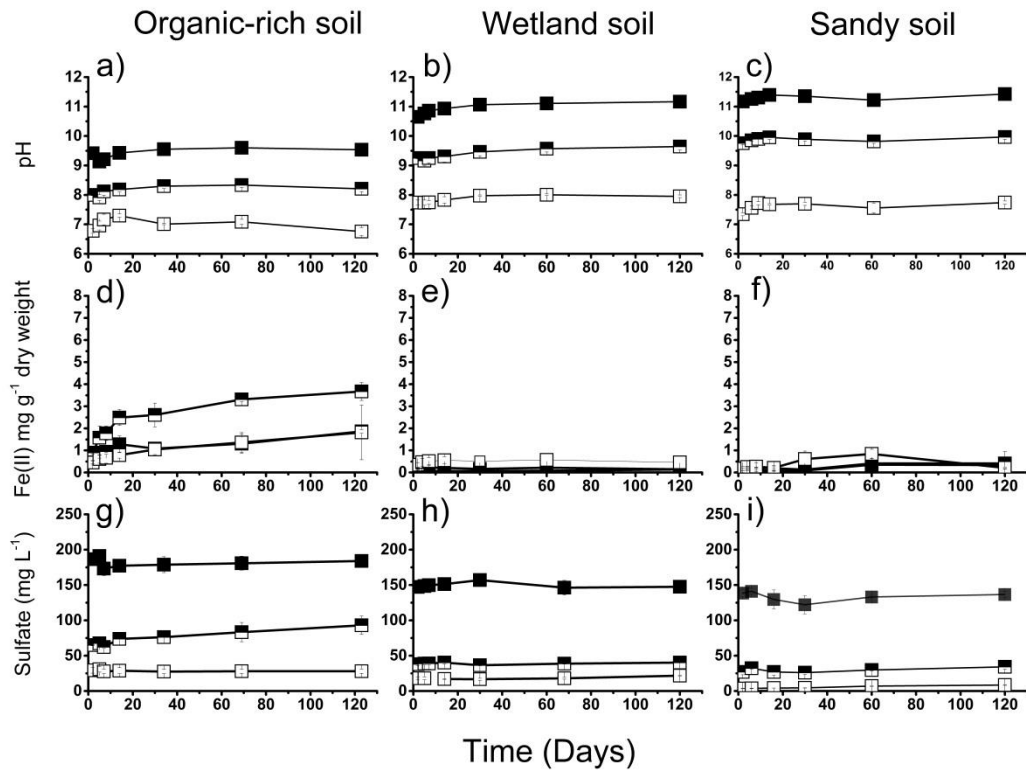


Figure S6. Geochemical analysis time plots from heat treated controls showing pH, Fe(II) mg g⁻¹ dry weight and SO₄²⁻. Empty squares = unamended, Half squares = 9% RM addition, Full squares = 33% RM addition. Error bars are 1 σ of triplicate results (where not shown, errors are within the symbol size).

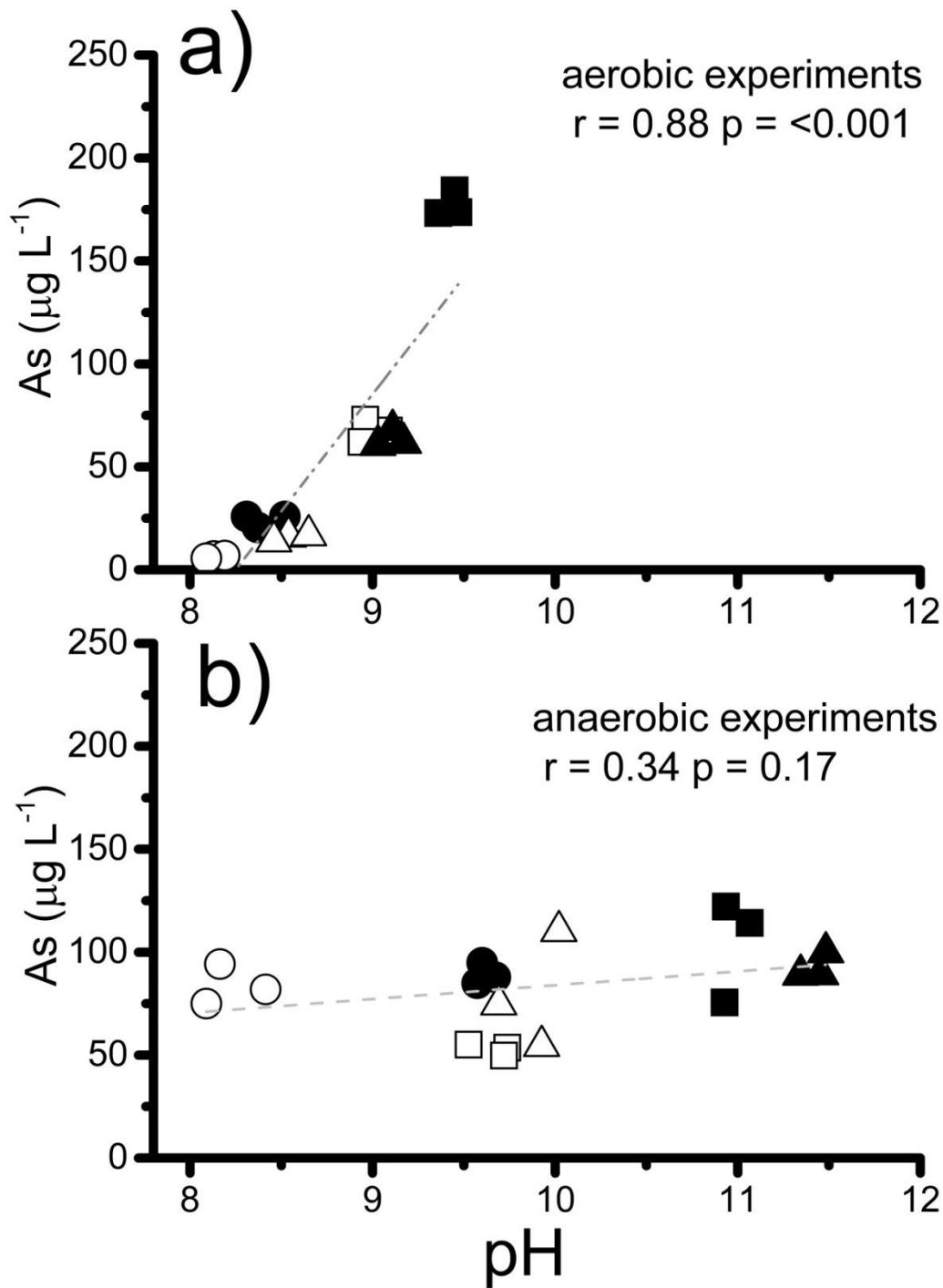


Figure S7. As concentration vs pH at the both the aerobic (a) and anaerobic (b) red mud experiments at the incubation end point. There is no significant correlation present (Pearson's correlation) in the anaerobic experiments but there is a positive correlation present in the aerobic experiments. The dotted lines indicate the highest and lowest concentrations determined from individual red mud amended microcosms. Full symbols = 33% RM addition, Empty symbols = 9% RM addition, Circles = Organic-rich soil, Squares = Wetland soil and Triangles = Sandy soil.

References

- Binsted, N., 1998. CLRC Daresbury Laboratory EXCURV98 program. CLRC Daresbury Laboratory, Warrington, UK.
- Binsted, N., Strange, R.W., Hasnain, S.S., 1992. Constrained and Restrained Refinement in EXAFS Data-Analysis with Curved Wave Theory. *Biochemistry* 31, 12117-12125.
- Booth, C.H., Hu, Y.J., 2009. Confirmation of standard error analysis techniques applied to EXAFS using simulation., in: DiCiccio, A., Filipponi, A. (Eds.), 14th International Conference on X-Ray Absorption Fine Structure. Iop Publishing Ltd, Bristol.
- Charlet, L., Morin, G., Rose, J., Wang, Y.H., Auffan, M., Burnol, A., Fernandez-Martinez, A., 2011. Reactivity at (nano)particle-water interfaces, redox processes, and arsenic transport in the environment. *C. R. Geosci.* 343, 123-139.
- Gurman, S.J., Binsted, N., Ross, I., 1984. A RAPID, EXACT CURVED-WAVE THEORY FOR EXAFS CALCULATIONS. *Journal of Physics C-Solid State Physics* 17, 143-151.
- Mayes, W.M., Jarvis, A.P., Burke, I.T., Walton, M., Feigl, V., Klebercz, O., Gruiz, K., 2011. Dispersal and Attenuation of Trace Contaminants Downstream of the Ajka Bauxite Residue (Red Mud) Depository Failure, Hungary. *Environmental Science & Technology* 45, 5147-5155.
- Morin, G., Ona-Nguema, G., Wang, Y.H., Menguy, N., Juillot, F., Proux, O., Guyot, F., Calas, G., Brown, G.E., 2008. Extended X-ray absorption fine structure analysis of arsenite and arsenate adsorption on maghemite. *Environmental Science & Technology* 42, 2361-2366.
- Peacock, C.L., 2009. Physicochemical controls on the crystal-chemistry of Ni in birnessite: Genetic implications for ferromanganese precipitates. *Geochim. Cosmochim. Acta* 73, 3568-3578.
- Ravel, B., Newville, M., 2005. ATHENA, ARTEMIS, HEPHAESTUS: data analysis for X-ray absorption spectroscopy using IFEFFIT. *J. Synchrot. Radiat.* 12, 537-541.
- Tenderholt, A., Hedman, B., Hodgson, K.O., 2007. PySpline: A modern, cross-platform program for the processing of raw averaged XAS edge and EXAFS data, in: Hedman, B., Painetta, P. (Eds.), *X-Ray Absorption Fine Structure-XAFS13*, pp. 105-107.
- Tomic, S.S., B. G.; Wander, A.; Harrison, N. M.; Dent, A. J.; Mosselmans, J. F. W.; Inglesfield, J. E., 2005. New Tools for the Analysis of EXAFS: The DL_EXCURV Package, CCLRC Technical Report DL-TR-2005-01, Daresbury, UK.